Mesoscale Modal Coupling

JAMES C. McWILLIAMS

National Center for Atmospheric Research,[1] Boulder, CO 80307

COLIN Y. SHEN

Department of Oceanography, University of Washington, Seattle 98105

(Manuscript received 7 August 1979, in final form 22 January 1980)

ABSTRACT

Observations of mesoscale ocean eddies from the 1973 Mid-Ocean Dynamics Experiment (MODE) are used to calculate, by objective analysis, the modal coefficients, which are functions of horizontal position and time, in a representation based on the two most energetic vertical modes—the barotropic and first baroclinic. The gross energy levels associated with these modes are calculated and found to be generally consistent with previous estimates. Modal coupling statistics are also estimated: these are the volume integral modal energy exchange rate and the spatially lagged covariances between modal streamfunction and velocity fields. The former is found to be approximately zero and the latter have significant extrema at lag distances comparable to an eddy radius. Furthermore, the dominant contribution to these coupling signals comes from the time-averaged (over a little more than two months) mesoscale field, which from lengthy moored observations we can identify as an instantaneous realization of the very low frequency "secular scale" described by Schmitz (1978). Forecasts from this observational representation in a two-mode, quasi-geostrophic numerical model with no horizontal energy flux into the region of interest (an extreme statement of our observational ignorance of mesoscale processes outside the MODE region) consistently fail to preserve either these covariance relations or the secular scale mesoscale component for any significant time, with a possible exception of the zero energy transfer rate in a small [~(100 km)^2], data dense region for a brief time (~10–15 days). Since these forecast failures occur on a time short compared to a turbulent predictability time, it is proposed that a missing, and observationally undocumented, process of exterior influence (such as radiation from the Gulf Stream region) is probably required to adequately model the mesoscale modal coupling in the MODE region.

1. Introduction

Frequently, if not generally, mid-ocean mesoscale currents have the greater part of their energy in a few vertical modes, with relatively large vertical length scales (Bernstein and White, 1974; Davis, 1975; McWilliams, 1976; Pochapsky, 1976; Richman *et al.*, 1977; Rossby, 1974; Rossby and Sanford, 1976). Furthermore, these modes are similar in many ways to the theoretical modes for linear quasi-geostrophic waves. McWilliams and Flierl (1975) showed that the first two empirical orthogonal modes of Davis (1975)—which contained 92% of the depth integrated velocity variance from current meter observations between 400 m and the bottom during the Mid-Ocean Dynamics Experiment (MODE)—were each accurately represented as a linear combination of the barotropic and first baroclinic theoretical modes for a flat ocean bottom and no mean current. The fact that linear combinations were required, however, indicates that the two modes are correlated, rather than independent as linear theory would suggest.

The purposes of this paper are to further explore the coupling between the theoretical modes and to assess our understanding of its implications through numerical model forecasts. The data base used here is also from MODE: as described in McWilliams (1976), geostrophic streamfunction is calculated by objective analysis from SOFAR float trajectories and STD/CTD profiles. Several types of modal statistical relations are estimated from these data, including the volume-averaged modal energy exchange rate and spatially lagged covariances for streamfunction and velocity. Forecasts from these data are made in a two-mode quasi-geostrophic model which is similar to ones frequently used in the past (e.g., Rhines, 1977). The forecasts are evaluated primarily through the degree to which they preserve these observed modal relations.

[1] The National Center for Atmospheric Research is sponsored by The National Science Foundation.

0022-3670/80/050741-12$07.00

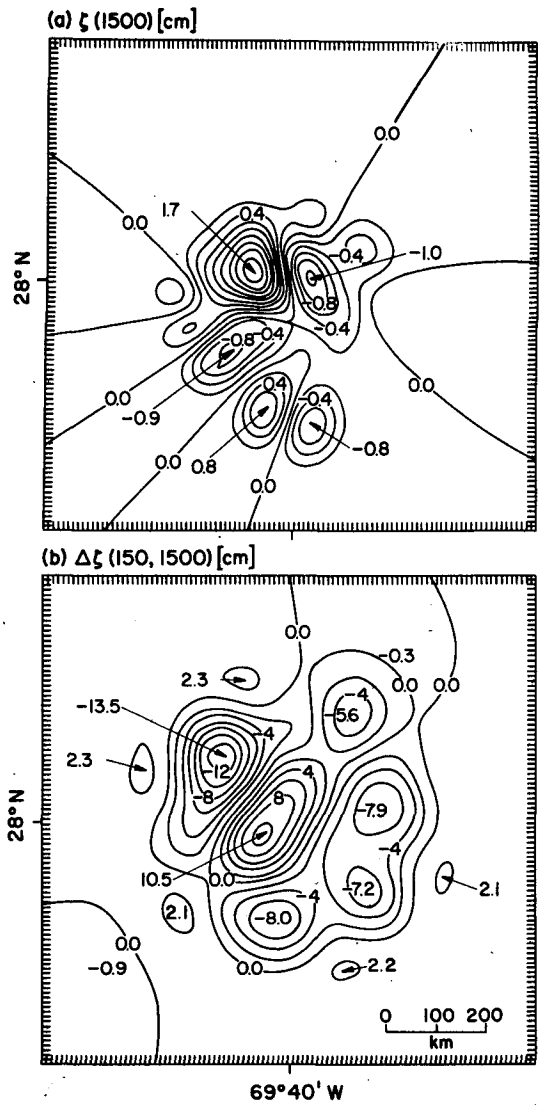

FIG. 1. Objective analyses of dynamic pressure head fields for year day 140 of 1973. The domain is (1000 km)², centered on 28°N, 69°40'W, with a grid resolution of 10 km. The contour interval is 0.2 for ζ(1500) and 2.0 for Δζ(150, 1500).

2. The data

The data preparation is similar to that described in McWilliams (1976). From observations of velocity at 1500 m depth (displacement rates of neutrally buoyant SOFAR floats) and dynamic heights between 1500 and 150 m (from STD or CTD profiles), the dynamic pressure heads (cm) ζ(1500) and Δζ(150, 1500) are estimated by the technique of objective analysis. No time and horizontal mean currents are assumed [this is in contrast with the treatment of ζ(1500) in McWilliams (1976)]. These fields are estimated on a regular grid (of spacing 10 km and extent 1000 km, centered as was MODE at 28°N, 69°40'W) for compatability with numerical model forecasts. Observations in a 5-day interval are combined. There were 10 such intervals during MODE when data were plentiful (defined as having at least 10 floats and 40 profiles); these are centered at year days 100, 105, 110, 130, 135, 140, 145, 155, 160 and 165 of 1973. This data set is referred to as the total one (T). A subset of greater data quantity (designated Q), having at least 12 floats and 50 profiles, includes year days 130, 135, 140, 145, 165; obviously any advantage gained from Q compared to T, because the individual interval estimates are more accurate, will be partially lost because of the fewer intervals, or realizations, available. A time mean mesoscale field (designated M) is a simple average over each of the 10 intervals of T. An alternative estimate of the mean (designated U) is constructed from days of greater data quantity and has weights which reduce the bias of the nonuniform (in time) occurrence of the intervals in T. It is a linear combination of days 105 and 165, with weight factor one-third, and days 135, 140, and 145 with weight factor one-ninth.

An example of ζ(1500) and Δζ(150, 1500) for day 140 is shown in Fig. 1. The consequence of objective analysis with covariance functions which decay to zero for large spatial lags is apparent: away from observations—almost all of which occur in the central (300 km)² of the domain—the dynamic pressures become small. They are effectively zero at the domain boundaries. There is a high degree of physical nonsense in such a specification because one is removing the influence of the rest of the ocean, mesoscale and mean currents both, on the particular region where observations are available. However, for diagnostic or forecast studies such as this one, specifying artificial exterior or boundary data would impose dynamical prejudices, certainly on the model forecasts and partly on the initial data, which could obscure the modal coupling relations in the data. The purpose here is not to make the best forecasts, but to make use of forecasts as an interpretive tool.

Also of interest are plots of the time mean fields in Fig. 2. One can see first that there is little difference between the M and U estimates and second that there are qualitative similarities between the mean fields in Fig. 2 and the instantaneous ones in Fig. 1. Furthermore, the extrema in the mean are generally more than half as large as their instantaneous counterparts. Thus, a significant amount of the mesoscale energy resided in the mean in MODE. Yet, we know from much longer time series (Schmitz, 1977; Freeland *et al.*, 1975; Tarbell and Spencer, 1978) that the true means are quite small in this region. Thus, the MODE mean fields are in fact a realization of very low-frequency mesoscale currents, which Schmitz (1978) has termed the "secular scale." Note that the currents associated

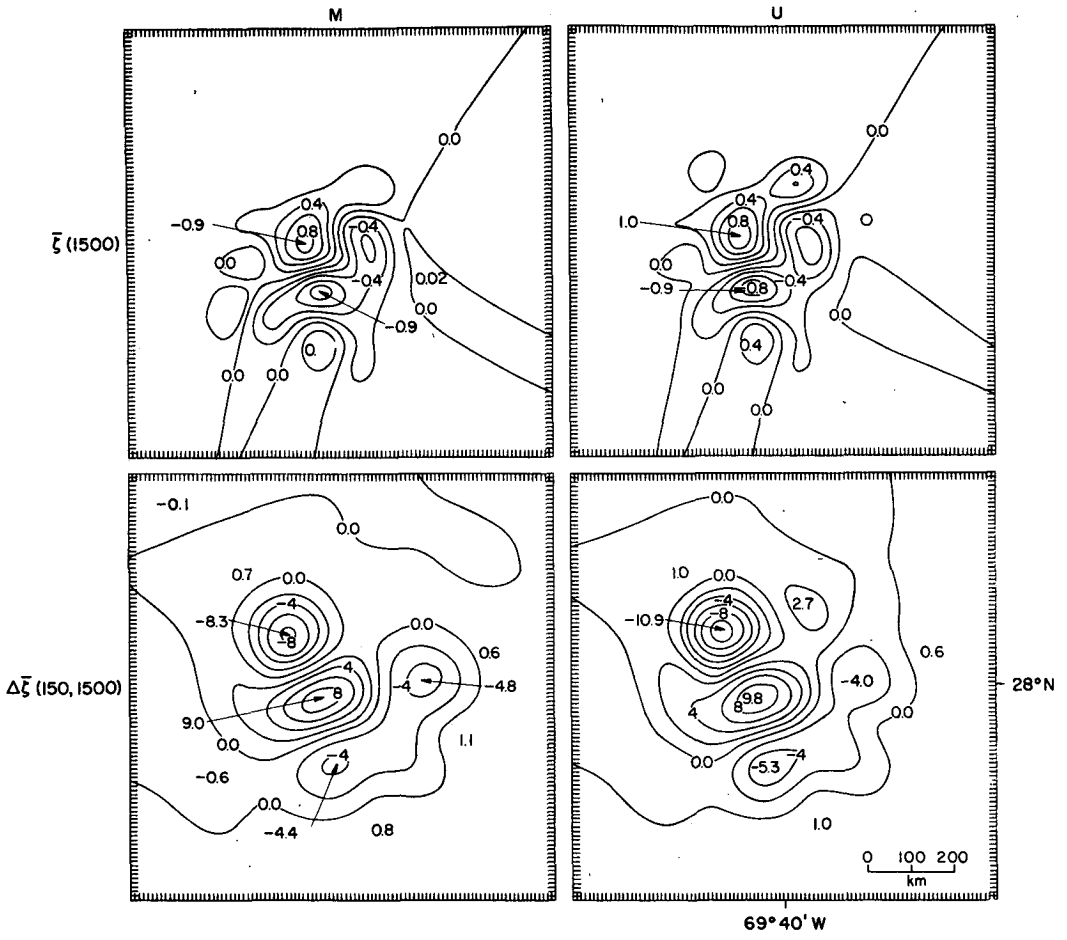

FIG. 2. Time averaged dynamic pressure heads (cm) for the two months of MODE. M and U are variants of the averaging defined in the text. The contour intervals are 0.2 for $\bar{\zeta}(1500)$ and 2.0 for $\Delta\bar{\zeta}(150, 1500)$.

with the mean have a more east-west alignment than do the instantaneous ones; this is a feature previously noted from mooring observations (Richman *et al.*, 1977) for this region.

3. The vertical modes

We shall adopt a representation for the geostrophic streamfunction $\Psi(x,y,z,t)$ as a linear combination of the barotropic and first baroclinic vertical modes, i.e.,

$$\Psi = \psi(x,y,t)F_1(z) + \chi(x,y,t)F_2(z). \qquad (1)$$

The modal functions F_j are calculated from linear, quasi-geostrophic theory assuming the ocean bottom is flat. The barotropic mode is a constant with depth, $F_1(z) = 1$, in the absence of mean horizontal currents, and it is approximately the same constant for the weak mean currents of the MODE region. The baroclinic mode, however, is significantly influenced by the presence of a surface intensified mean zonal current. This is shown in Fig. 3, which is based upon calculations described in McWilliams (1976). We shall use a superscript u to indicate quantities calculated from $F_2(z)$ with $\bar{u}(z) \neq 0$ and a superscript 0 for F_2 with $\bar{u} \equiv 0$.

The mesoscale modal coefficients will be calculated by superposition of the pressure heads defined in Section 2, *viz.*,

$$\begin{pmatrix} \psi \\ \chi \end{pmatrix} = A \begin{pmatrix} \zeta(1500) \\ \Delta\zeta(150, 1500) \end{pmatrix}, \qquad (2)$$

where A is a 2×2 superposition matrix.

We shall make use of nondimensional modal streamfunctions, based upon the product of a velocity V_0 and a horizontal length L_0 (we choose values of 5 cm s^{-1} and 60 km, respectively, as representative of square root of velocity variance and zero crossing of the transverse velocity covariance function—see McWilliams and Owens (1976). The corresponding dimensionalizing factor for pressure head is $V_0L_0f_0/g$, where f_0 is the local Coriolis frequency (0.7×10^{-4} s^{-1}) and g the gravitational acceleration

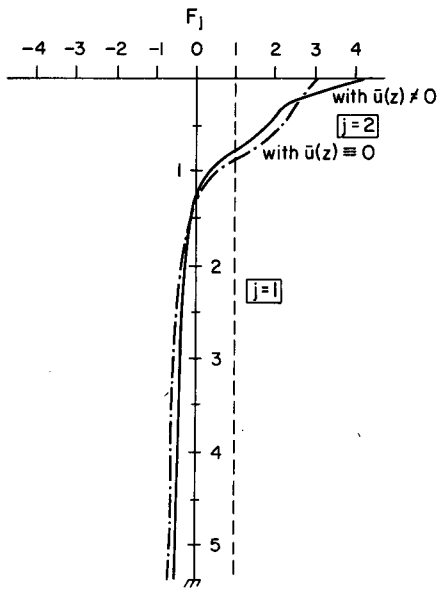

FIG. 3. The first two linear theoretical modes: $j = 1$ corresponds to the barotropic mode and $j = 2$ to the first baroclinic mode. Two variants of the latter are shown. The modes are orthonormal, $H^{-1} \int_H^0 dz\ F_i(z)F_j(z) = \delta_{ij}$. (From McWilliams, 1976).

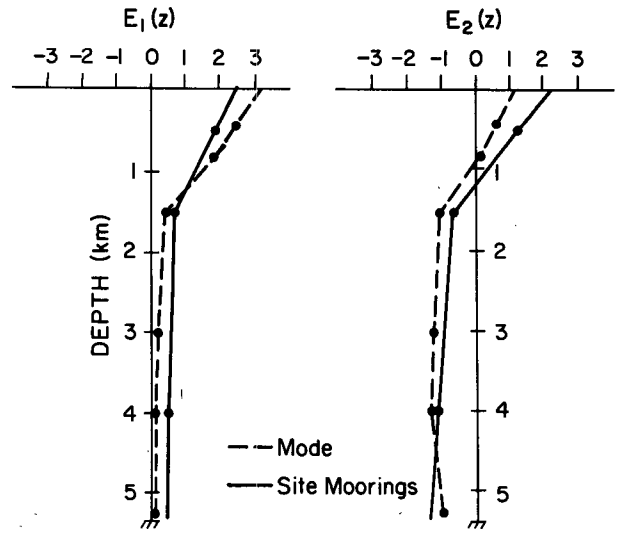

FIG. 4. The empirical orthogonal modes for velocities measured from moored current meters. Vertical axis is depth in kilometers.

constant (9.8 m s^{-2}). To a first approximation A is a diagonal [$\Delta\zeta$ reflects no contribution from the constant $F_1(z)$ and 1500 m is close to the depth where $F_2(z) = 0$]. For orthonormal modes, the superposition matrix in this diagonal approximation is given by

$$\left.\begin{aligned} A_{11} &= (g/V_0 f_0 L_0)F_1(1500)^{-1} \\ A_{22} &= (g/V_0 f_0 L_0)[F_2(150) - F_2(1500)]^{-1} \\ A_{12} &= A_{21} = 0 \end{aligned}\right\} . \quad (3)$$

For the numbers listed above and the $F_j(z)$ in Fig. 3, $A_{11} = 0.47$ and $A_{22}^0 = 0.17$ and $A_{22}^u = 0.14$. A more accurate approximation results from $A_{12} \neq 0$, since $F_2(1500) \neq 0$, *viz.*,

$$A_{12} = -\frac{F_2(1500)}{F_1(1500)} A_{22}, \quad (4)$$

which has the numerical values of $A_{12}^0 = 0.03$ and $A_{12}^u = 0.02$. Since these values are so small, most of the following calculations will make use of equations (3).

Vertical modes can alternatively be represented as empirical orthogonal functions $E_j(z)$, whose properties are discussed in Davis (1977), for example. They can be represented as a combination of the theoretical modes plus a residual, i.e.,

$$E_j(z) = \sum_k B_{jk}F_k(z) + \nu_j(z). \quad (5)$$

The modes E_j and F_k are each orthonormal and complete, at whatever resolution in z is available; thus, if the full sets were retained, the residual would vanish. However, for our truncated two-mode representation (in both E_j and F_k), $\nu_j \neq 0$ for any vertical resolution beyond two levels.

Davis (1975) calculated the $E_j(z)$ from the MODE moored current meter data set with six levels between ~450 and 5000 m depth. We have repeated his calculations with perhaps slight differences in the vertical discretization required to approximate the vertical integral involved in the calculation (N.B., this integral is defined in the caption to Fig. 3). We find that 94% of the depth-averaged velocity variance can be accounted for in the first two $E_j(z)$. A similar calculation has been made from the MODE region site mooring, with 96% of the variance in the first two modes. These site mooring data are of coarser resolution (three levels between ~500 and 4000 m depth) but of much greater duration (covariance pairs could be calculated for time intervals between 430 and 640 days in length), and hence presumably more typical of average mesoscale conditions.[2]

Plots of $E_j, j = 1$ and 2, for the two mooring data sets, are shown in Fig. 4 and various properties of this representation are shown in Table 1. Results from the two data sets are generally similar in the modal shapes and the distribution of variance between them. The residuals from (5) are small in rms depth average, indicating that the two-mode empirical and theoretical representations are effectively equivalent. Table 1 includes depth-averaged kinetic energies K_j associated with the theoretical

[2] The site mooring data are described in Tarbell and Spencer (1978); covariance pairs were provided to the authors by courtesy of Dr. William Schmitz.

modes, their ratio, and the velocity correlation coefficient between the theoretical modes

$$C_v \equiv \langle \nabla\psi \cdot \nabla\chi \rangle [\langle \nabla\psi \cdot \nabla\psi \rangle^{1/2} \langle \nabla\chi \cdot \nabla\chi \rangle^{1/2}]^{-1}, \quad (6)$$

where the angle brackets denote averages over the data set. The extended duration data set had a relatively higher fraction of barotropic kinetic energy than MODE and the modal correlation coefficient was smaller, though still significantly nonzero.

The kinetic energy values from current meters can be compared with ones from the float and STD/CTD data during MODE. There is approximate, but by no means precise, overlap in space and time between them and the MODE current meter data. The energy values for the theoretical modes can be taken from Section 5 of McWilliams (1976), with an additional multiplication by $(1 - \epsilon_*^2)$, where ϵ_*^2 is the irreducible noise variance in a point measurement (listed in Table 3 of McWilliams, 1976), in order to convert total energy to mesoscale energy. The current meter measurements are typically low-pass time filtered and are thus more comparable to the latter. The results are

$$\left.\begin{aligned} K_1 &= 9.4 \text{ cm}^2 \text{ s}^{-2} \\ K_2 &= 18.2 \text{ cm}^2 \text{ s}^{-2} \\ K_1/K_2 &= 0.5 \end{aligned}\right\} . \quad (7)$$

These compare reasonably well with the MODE values of Table 1, if we identify K_2 here with K_2^u instead of K_2^0 [N.B., Fig. 8 of McWilliams, (1976) indicates that F_2^u is more consistent with the MODE hydrographic observations than is F_2^0]. If we further make a correction for baroclinic mode contributions to 1500 m float variance, similar to the one made in Eq. (4), then K_1 is reduced from its value in Eq. (7) by ~ 1 cm^2 s^{-2}, which further improves the comparison with Table 1.[3]

In summary, most of the mesoscale energy in the MODE region resides in two vertical modes, these vertical modes are consistent with the representation (1), the modes are correlated in velocity at zero spatial lag, and the modal kinetic energies during MODE can be consistently estimated from independent data sets.

4. Modal coupling relations

In addition to the modal velocity correlation (6) examined in the previous section, we shall make estimates of three further modal coupling statistical quantities. Two are the spatially lagged correlations between streamfunction and velocity:

$$\left.\begin{aligned} C_\psi(\mathbf{r}) &= \frac{\int\int_R \psi(\mathbf{x})\chi(\mathbf{x}+\mathbf{r})d\mathbf{x}}{\left[\int\int_R \psi(\mathbf{x})^2 d\mathbf{x} \int\int_R \chi(\mathbf{x}+\mathbf{r})^2 d\mathbf{x}\right]^{1/2}} \\ C_v(\mathbf{r}) &= \frac{\int\int_R \nabla\psi(\mathbf{x})\cdot\nabla\chi(\mathbf{x}+\mathbf{r})d\mathbf{x}}{\left[\int\int_R \nabla\psi(\mathbf{x})^2 d\mathbf{x} \int\int_R \nabla\chi(\mathbf{x}+\mathbf{r})^2 d\mathbf{x}\right]^{1/2}} \end{aligned}\right\} , \quad (8)$$

where $\mathbf{x} = (x,y)$ and R is the region in $\mathbf{x}$ over which the integrations are made. $\mathbf{r}$ is the lag vector. Note that $C_v(0)$ is equivalent to C_v from (6) except for differences in averaging. The third quantity, which has a more direct dynamical interpretation than (8), is the nondimensional, volume-averaged, modal energy exchange rate

$$\epsilon = -Q_* \int\int_R d\mathbf{x}\psi J(\chi, \nabla^2\chi)/\text{area } (R). \quad (9)$$

A derivation of (9) is given in Section 4 of McWilliams and Flierl (1979). Positive values of ϵ imply a transfer of first baroclinic mode energy to barotropic mode energy. The parameter Q_* is defined as $V_0/(\beta L_0^2)$ in a nondimensionalization where, in addition to the quantities described following Eq. (2), the time scale is that for Rossby waves, $(\beta L_0)^{-1}$. Here β is the northward gradient of the Coriolis frequency and has the value 2×10^{-11} m^{-1} s^{-1} for the MODE latitude; consequently, Q_* has the value 0.7. ϵ can be made dimensional by multiplying by $\beta V^2 L_0$ ($=3 \times 10^{-5}$ cm^2 s^{-3}). Note from (3) and (4) that $\epsilon \propto A_{11}A_{22}^2$ and that ϵ is insensi-

TABLE 1. Current meter empirical orthogonal function properties.

	MODE	Site moorings
Variance (cm^2 s^{-2})	39	34
Fractional variance in $E_1, E_2, \ldots$	0.73, 0.21, . . .	0.69, 0.27, . . .
B_{11}	0.60	0.83
B_{21}	0.80	0.54
B_{12}^0, B_{12}^u	0.80, 0.98	0.55, 0.67
B_{22}^0, B_{22}^u	−0.61, −0.74	−0.83, −1.01
rms (in z) ν_1, ν_2	0.08, 0.14	0.03, 0.10
K_1 (cm^2 s^{-2})	8.0	9.4
K_2^0, K_2^u (cm^2 s^{-2})	10.9, 16.2	6.7, 10.0
$K_1/K_2^0, K_1/K_2^u$	0.7, 0.5	1.4, 0.9
C_v	0.6	0.4

[3] The formula involved in the correction is

$$[1 - \epsilon_*^2(1500)]K_{1500} = K_1F_1(1500)^2 + K_2F_2(1500)^2 + 2\sqrt{K_1K_2}F_1(1500)F_2(1500)C_v,$$

This yields a correction to K_1, of the size stated above, when we use $C_v = 0.2$ as estimated from the float and CTD/STD data set (see Section 4).

TABLE 2. $C_\psi(0)$ and its variability.

Lateral dimension of R (km)	Data sets			
	T	Q	M	U
1000	−0.01 [0.11]*	0.00 [0.15]*	0.10	0.07
500	0.01 [0.11]	0.10 [0.15]	0.11	0.08
300	−0.00 [0.11]	0.03 [0.12]	0.16	0.16
140	0.03 [0.27]	0.16 [0.25]	0.10	0.05
140**	0.14 [0.24]	0.18 [0.20]	0.05	−0.02

* For the data sets T and Q, the unbracketed number is the average value of $C_\psi(0)$ over the set of component intervals and the bracketed number is rms deviation from the average.

** Rather than centered at 28°N, 69°40′W, as are all of the other square regions R, this one is displaced 40 km in, arbitrarily, the southward direction.

tive to $A_{12} \neq 0$ (insofar as the boundaries of R are taken either along streamlines in χ or where the velocities are small). For the ϵ estimates of this section, we shall adopt the approximation (3) and use $A_{22} = A_{22}^0 = 0.17$.

We first consider the zero lag correlations. Tables 2 and 3 list a number of different estimates of $C_\psi(0)$ and $C_v(0)$, based on different regions R and data sets T, Q, M and U (see Section 2 for their definitions). The variety of estimates seems appropriate because there are competing effects influencing the accuracy of the estimates: larger data sets [e.g., larger area (R) or T instead of Q] have more mesoscale realizations but have lower accuracy on average in point values of ψ and χ, and vice versa. In addition, correlation estimates for the mean fields M and U are included because the very low frequency mesoscale component will be shown below to play an important role in the observed modal coupling. For data sets T and Q, rms variations about the mean estimate are also listed; when divided by $N^{1/2}$, where N is the number of degrees of freedom in the estimate, the rms can be taken as the uncertainty in the mean.

Values for $C_\psi(0)$ are generally small but positive in Table 2. For data sets T and Q, $C_\psi(0)$ increases as R shrinks; however, for the smallest regions the uncertainty increases as well. If we take $N = 10$ for T and $N = 5$ for Q, which yield least possible values for the uncertainties, then one can summarize Table 2 as implying $C_\psi(0) \approx 0.1$ with an uncertainty of the same size.

TABLE 3. $C_v(0)$ and its variability.

Lateral dimension of R (km)	Data sets			
	T	Q	M	U
1000	0.03 [0.11]*	0.00 [0.11]*	0.12	0.10
500	0.04 [0.12]	0.02 [0.12]	0.14	0.12
300	0.09 [0.12]	0.07 [0.13]	0.23	0.26
140	0.15 [0.16]	0.16 [0.10]	0.40	0.41
140**	0.30 [0.11]	0.28 [0.12]	0.59	0.55

* As in Footnote 1 to Table 2 except for $C_v(0)$.

** As in Footnote 2 to Table 2.

TABLE 4. $100 \times \epsilon$ and its variability.

Lateral dimension of R (km)	Data sets			
	T	Q	M	U
1000	−0.03 [0.32]*	0.01 [0.4]*	0.00	0.03
500	−0.15 [1.3]	−0.01 [1.4]	0.01	0.15
300	−0.63 [3.3]	−0.29 [4.0]	0.50	0.93
140	−1.13 [5.4]	−1.92 [6.7]	−0.16	−3.02
140**	0.32 [2.8]	0.50 [2.1]	1.35	0.42

* As in Footnote 1 to Table 2 except for ϵ.

** As in Footnote 2 to Table 2.

The values for $C_v(0)$ in Table 3 are consistently larger than those for $C_\psi(0)$ both on average and for the mean fields, while the correlation uncertainties are no larger and perhaps slightly smaller for velocity. A summary value for $C_v(0)$ would be +0.2, with an uncertainty less than ±0.1. For the mean fields the zero lag velocity correlation is larger, ~0.5. The present value 0.2 can be compared with the values 0.4 and 0.6 from the moored measurements in Table 1. The fact that it is smaller, while probably influenced by differences in the mesoscale realizations sampled in the different data sets, is partly because both of the current meter data sets are of longer duration than the two-month float and density data set. Hence more of the secular scale, with its higher $C_v(0)$, contributes to the total correlation. It is also partly because the moored measurements were made at zero spatial lag, while the float and CTD/STD measurements were not and their $C_v(0)$ estimate is only arrived at by interpolation between measurements. The objective analysis interpolation assumes no modal correlation [at least for the Eq. (3) approximation], which is why both $C_\psi(0)$ and $C_v(0)$ decrease as R is expanded to include data sparse areas. As we shall see below, the extrema in C_ψ and C_v do not occur at zero lag, and it is reasonable to interpret the present zero lag underestimate as a blurring of $C_v(\mathbf{r})$ structure near $\mathbf{r} = 0$. Note that because A_{12} is positive, the approximation (4) would yield slightly larger $C_\psi(0)$ and $C_v(0)$ values than the present ones with (3).

Estimates of the modal energy transfer rate from (9) are listed in Table 4. Here one can see that the estimates from T and Q are consistently smaller than their uncertainties, while from M and U the estimates are no larger than those of T and Q and have considerable scatter as the region R is changed. In contrast to the normalized correlation estimates,

an increase in ϵ values and their uncertainties is to be expected as R shrinks simply due to an exclusion of data sparse areas where ψ and χ are small. We can conclude, therefore, that during the MODE experiment the modal energy transfer was insignificantly different from zero; in Section 5 we shall see that the observed ϵ values are also generally much smaller than those calculated by the models 10 or 20 days after initialization.

Finally, we examine the spatially lagged structure of the correlations (8). Fig. 5 shows them for data sets T and Q, and Fig. 6 shows them for the MODE average fields M (U is unimportantly different from M in this regard). In each of these calculations, the averaging region R is held constant as a square 300 km on a side. Note the following features: Barotropic streamfunction or velocity structures are correlated with baroclinic ones lying 50–100 km to the southeast (with positive correlations) or northwest (with negative correlation). The largest streamfunction correlations are stronger than the velocity ones, which is the reverse of their relationship at zero lag (which is not an extremum in either covariance function). The correlations are somewhat larger in Q than T, indicating the necessity of high data quality for making these estimates accurately. The correlation values are considerably larger for the MODE mean mesoscale fields than for the total mesoscale field, although correlation patterns for the departures from the mean (not shown) are also similar to those in Figs. 5 and 6 but weaker.

In summary, then, there exist several clear modal coupling relations characterizing the mesoscale eddy realization in MODE. The barotropic and baroclinic modal fields are mutually aligned in such a way as to exchange no energy on average while being phase-locked with a spatial

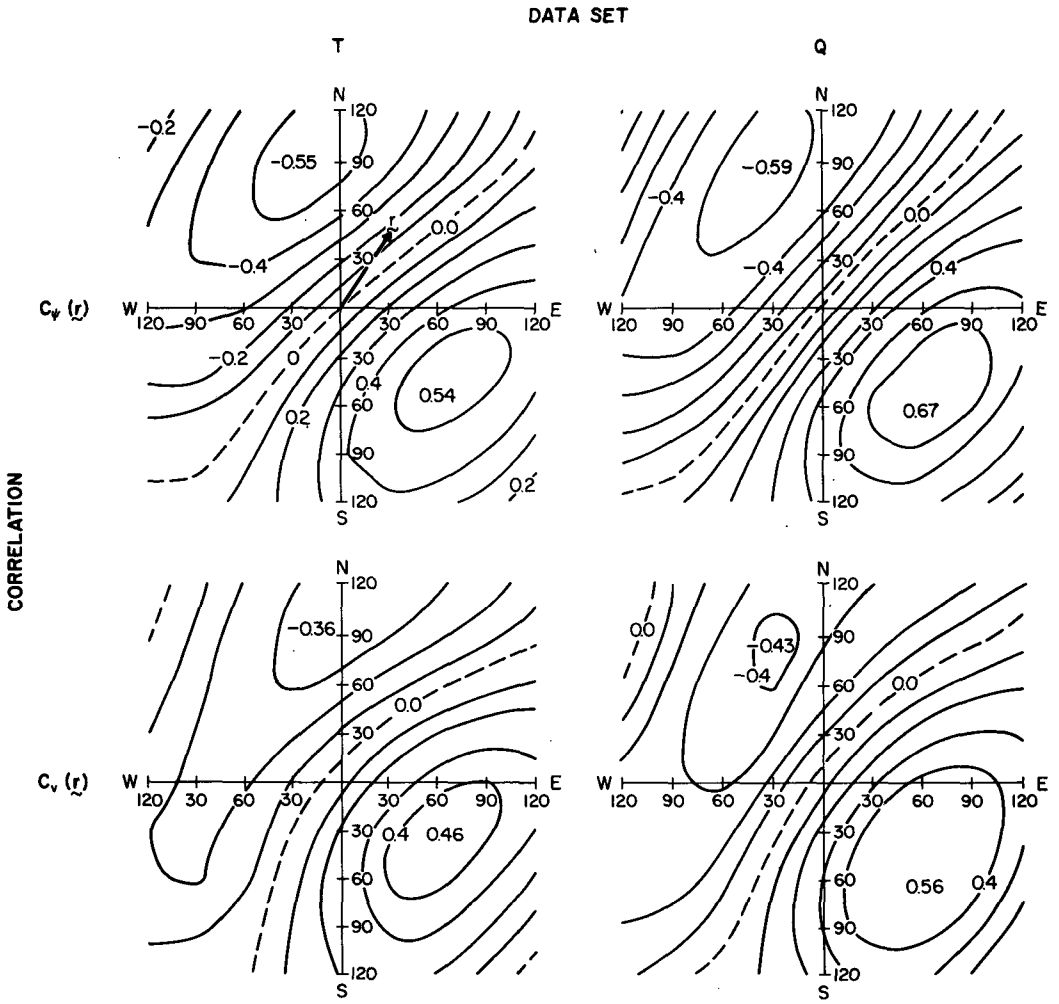

FIG. 5. Contours of the indicated lagged correlations (contour interval = 0.1).

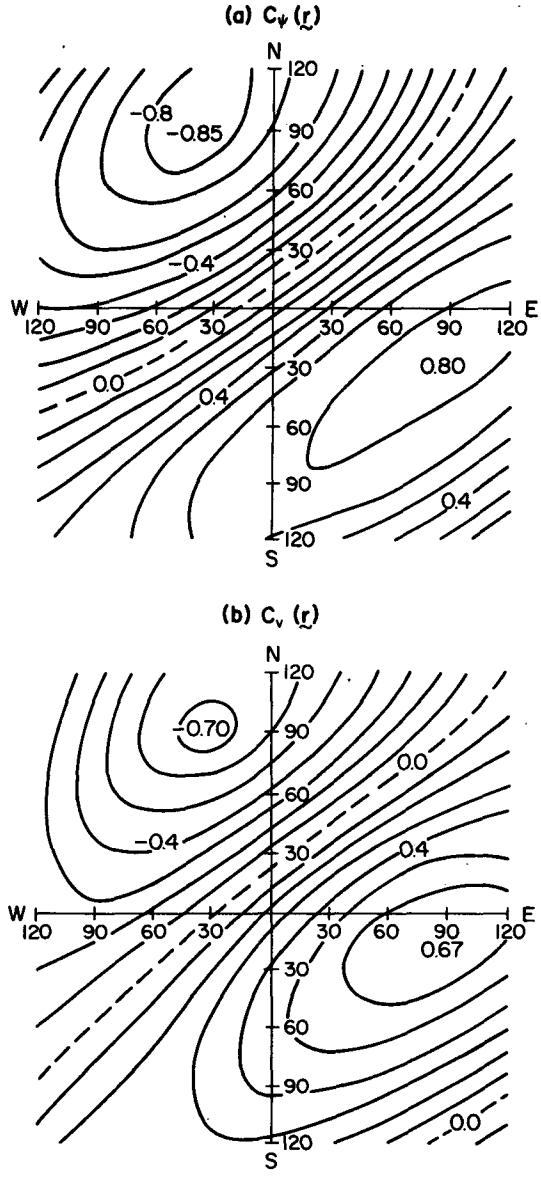

FIG. 6. Contours of streamfunction and velocity correlation functions for the MODE mean fields M (contour interval = 0.1).

shift between eddy centers. The lowest frequency mesoscale component exhibits these features most strongly.

5. Model forecasts

Forecasts have been made from initial data such as those shown in Fig. 1. The model used is one which is quasi-geostrophic, hydrostatic and adiabatic, and which is an orthonormal projection of the continuous physical equations by the two vertical modes of Eq. (1). The equations for this model have been derived and discussed in Flierl (1978) and McWilliams and Flierl (1979); they are

$$\left.\begin{aligned}
&\frac{\partial}{\partial t}\nabla^2\psi + \frac{\partial}{\partial x}\psi + Q_*[J(\psi,\nabla^2\psi) \\
&\quad + J(\chi,\nabla^2\chi)] + S[J(\psi,B) - \delta^{1/2}J(\chi,B)] \\
&\qquad - K\nabla^4\psi = 0 \\
&\frac{\partial}{\partial t}(\nabla^2 - \gamma^2)\chi + \frac{\partial}{\partial x}\chi + Q_*[\xi J(\chi,\nabla^2\chi) \\
&\quad + J(\psi,(\nabla^2 - \gamma^2)\chi) + J(\chi,\nabla^2\psi)] \\
&- S\delta^{1/2}[J(\psi,B) - \delta^{1/2}J(\chi,B)] - K\nabla^4\chi = 0
\end{aligned}\right\}. \quad (10)$$

These equations have been made nondimensional by the scales discussed following Eqs. (2) and (9), as well as B_0 as a characteristic height of the bottom topographic elevation $B(x,y)$ and H_0 as the mean depth of the ocean. The parameters of Eqs. (10) include

$$\gamma = L_0/R, \quad Q_* = V_0/\beta L_0^2, \quad S = B_0 f_0/\beta L_0 H_0, \quad K = \nu/\beta L_0^3, \quad (11)$$

where R is the internal deformation radius and ν the kinematic eddy viscosity. R, δ and ξ are parameters related to the basic stratification and rate of rotation (i.e., latitude). For the MODE region, we take

$$\left.\begin{aligned}
&R = 47 \text{ km}, \quad \delta = 0.16, \quad \xi = 2.10 \\
&\gamma = 1.3, \quad Q = 0.7, \\
&S = 5.9, \quad K = 0.0025
\end{aligned}\right\}. \quad (12)$$

The values (12) imply $B_0 = 550$ m and $\nu = 10^5$ cm^2 s^{-1}. The boundary conditions for (10) are periodicity in both x and y. For the domain in Fig. 1, the periodicity length is 1000 km; this is sufficiently larger than the initial region where ψ and χ are nontrivial so that the boundary influence on the solution (compared to one in an infinite domain) is slight for the length of forecast made.

An example of a forecast solution is shown in Fig. 7. Beginning from day 140 data (Fig. 1), a 25-day integration of (10) is made, with the end state to be compared to day 165 data. The ocean bottom is assumed flat ($S = 0$); otherwise the parameter values are (12). The initial fields for ψ and χ have been calculated with approximation (3); Eq. (2) is subsequently inverted after the integration to yield forecast dynamic pressure fields.

From Fig. 7 one can subjectively identify certain features. The barotropic field has expanded its nontrivial region in the model solution, primarily by the mechanism of barotropic Rossby wave radiation. This feature is missing in the day 165 observational representation because exterior region measurements were not made; however, if the ocean exterior were not quiescent, the net radiation

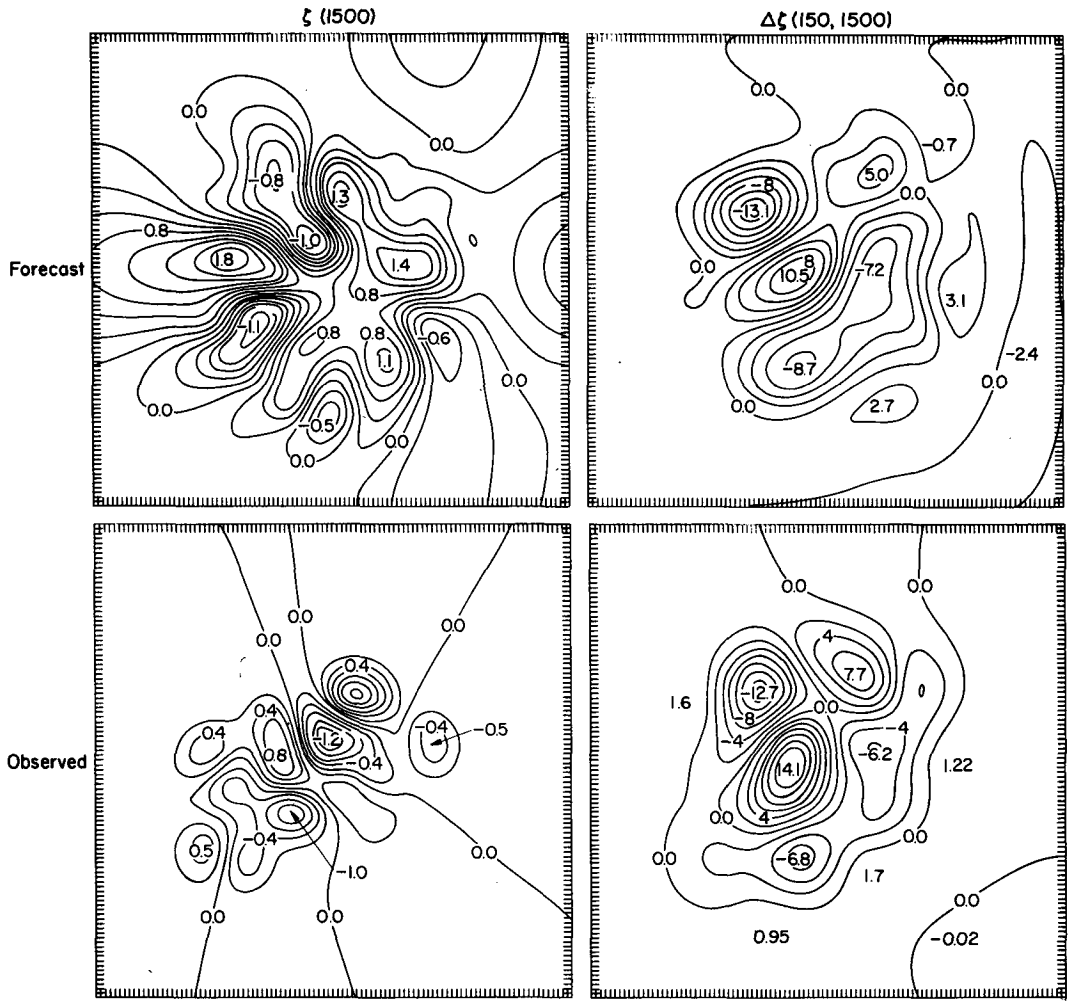

FIG. 7. Dynamic pressure head fields (cm) from a 25-day forecast with day 140 initial data (shown in Fig. 1) and from day 165 comparison data. Contour intervals are 0.2 for $\zeta(1500)$ and 2.0 for $\Delta\zeta(150, 1500)$.

would undoubtedly be less than in our model solutions. Another feature is the relative slowness of baroclinic changes compared to barotropic ones, both in the forecast and the observations. This is, of course, a frequently mentioned feature of mesoscale currents (Davis, 1975; Richman *et al.*, 1977; Schmitz, 1978), and it can be rationalized by the modal linear wave frequencies. However, we know from the modal correlations presented in Sections 3 and 4 that a significant component of each of the modal fields cannot have different time scales.

If one analyzes the changes in amplitude and position of various eddy centers in Fig. 7, a mixed impression of forecast skill is arrived at. For example, the baroclinic low-pressure center in the northwest sector weakened and moved slightly westward in the forecast; in fact, it did weaken, although about twice as much as forecast, and remained nearly stationary. A barotropic high-pressure center, not present in the initial data, appeared in the northeast sector in both the forecast and the observations; another new center, a barotropic low in the east, also appeared in the forecast but not quite in the location observed. The central baroclinic high was observed to intensify, whereas its amplitude remained constant in the forecast. Since the observational uncertainties in point values of the initial and final data fields are appreciable [~50 and 25% of typical extrema in $\zeta(1500)$ and $\Delta\zeta(150, 1500)$, respectively—see McWilliams (1976)], it is difficult to claim either any clear success or failure of the forecast from comparisons such as can be made visually from Fig. 7.

By reference to the modal coupling relations of Section 4, however, a clear judgment of forecast deficiency can be arrived at. Fig. 8 includes plots of each of $C_\psi(0)$, $C_v(0)$ and ϵ as functions of time for the 25-day forecast from year day 140 initial data. The zero-lag covariances develop negative values, with $C_\psi(0)$ more negative than $C_v(0)$, and the energy transfer rate ϵ systematically develops large positive values. All aspects of this behavior conflict with the

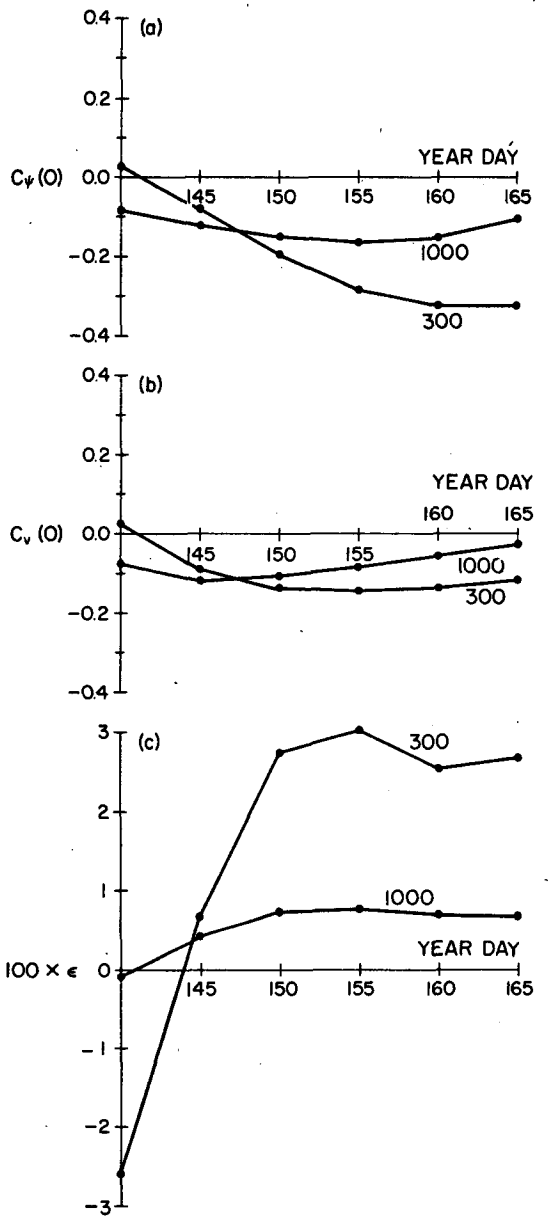

FIG. 8. Scalar modal coupling statistics from the 25 day forecast beginning on year day 140. The curve labels are the lateral dimensions in km for the integration region R.

observed average values of these quantities [i.e., $C_v(0) > C_\psi(0) \gtrsim 0$ and $\epsilon \approx 0$].

The day 140 forecast is only one realization and the above results are not necessarily typical. Nevertheless, when an ensemble of forecasts is made with each of the data fields in sets T or Q taken as initial data, the forecast deficiencies persist. This is illustrated in Table 5, where ϵ values and their uncertainties over the ensemble are listed for times 5 and 10 days after the beginning of the forecast for various integration domains R. In the initial data, ϵ is indistinguishable from zero in both T and Q for all R. Even after only 5 days of integration, however, ϵ assumes significantly positive values; the same is true, *a fortiori*, after 10 days. The only exception after 10 days occurs in the higher quality, fewer realization ensemble Q for the two, partially overlapping, small integration regions of lateral dimension 140 km. This exception must be viewed with skepticism, since the quantity of mesoscale realizations supporting it is unfortunately small. However, if one argues that the most probable explanation for the forecast deficiencies is the incorrect or inadequate incorporation of exterior region influence in the model, then this exception, where the region R is imbedded in a broader region of reasonably high quality initial data, is a plausible one: the outer regions of the MODE data can act, for a brief time, as an adequate exterior region for the small inner region R. Notice, though, the implications of such an interpretation. Not only must the initial data cover quite a large region in order to adequately forecast the modal coupling relations for intermediate periods of a month or so, but the data quality and sampling density must be quite good—at least as good as the best of MODE.

The various modal covariances also lose their observed characteristics over the ensemble of forecasts. The zero-lag values become indistinguishable from zero after 10 days of integration, with a weak suggestion of a tendency to develop negative values at later times. The lag-space covariances $C_\psi(\mathbf{r})$ and $C_v(\mathbf{r})$ lose the structures shown in Figs. 5 and 6. The time-invariant component of the initial data (Fig. 2) is not well preserved.

Of course, there are many other possible explanations for the modal coupling forecast failures besides that of a missing exterior region influence. The forecast model is based on a number of assumptions and particular parameter values [i.e., those in Eq. (12)] about which one can reasonably have doubts.

A number of additional forecasts have been made with the model equations (10), using alternative assumptions and parameter values. While appreciable changes in the forecast solutions resulted, the

TABLE 5. Ensemble forecasts of energy transfer rate.

Data set	N	Lateral dimension of R (km)	$100 \times (\epsilon \pm \text{rms}/N^{1/2})$ Time t_0	t_0 + 5 days	t_0 + 10 days
T	10	1000	−0.03 ± 0.10	0.35 ± 0.12	0.60 ± 0.12
		300	−0.6 ± 1.0	1.9 ± 0.9	3.2 ± 0.9
		140	−1.1 ± 1.7	0.2 ± 1.7	1.7 ± 1.4
		140*	0.3 ± 0.9	1.1 ± 1.3	2.1 ± 1.5
Q	5	1000	0.01 ± 0.17	0.45 ± 0.12	0.70 ± 0.09
		300	−0.3 ± 1.8	2.4 ± 1.2	3.4 ± 1.0
		140	−1.9 ± 3.0	−0.9 ± 2.7	−0.4 ± 1.6
		140*	0.5 ± 0.9	0.7 ± 0.9	0.5 ± 1.3

* As in Footnote 2 to Table 2.

deficiencies in the modal coupling relations were not significantly corrected. The forecast variants were the following: the values of A_{11} and A_{22} were independently altered by up to 100% of their values (3); A_{12} was made nonzero according to (4); δ was increased by 20% with ξ and R altered according to their two-layer model proportionalities [i.e., $(1 - \delta)/\delta^{1/2}$ and $\delta^{1/2}$, respectively]; the periodicity length (model domain dimension) was decreased to 500 km; and nonzero bottom topography was added with $S = 5.9$ as in (12) [the topographic form $B(x,y)$ was a slight alteration of that used in Owens and Bretherton (1978), which is only qualitatively similar to the MODE region topography]. Obviously, this list of alternative models is not an exhaustive one, nor do any of the alternatives plausibly incorporate the influence of the rest of the ocean (the exterior) upon the MODE mesoscale eddies. The only variant in this list which significantly alters the character of the exterior region is the reduction of the periodicity length to 500 km. As can be seen, for example, in Fig. 1, within a central square of this dimension the initial eddy field is not quiescent; hence by the assumption of periodicity nor is any exterior region. While (500 km)^2 is perhaps too large an area to contain initial data with an accurate representation of the modal coupling relations (N.B., Tables 2–4), any further reduction of dimension would greatly distort the mesoscale eddy physics. It does seem, however, that the exterior quiescence in the initial data is not by itself the fundamental cause of forecast failure to preserve (or develop) the observed modal coupling relations. There is a further possible difficulty which should be considered: forecasts in a turbulent fluid are intrinsically limited in their time of predictability, as has been discussed in meteorology by Thompson (1957), Lorenz (1969a, 1969b) and Leith and Kraichman (1972). One can crudely summarize predictability theory as indicating forecast failure due to subsynoptic initial data ignorance in a time on the order of an energetic eddy circulation time $2\pi L_0/V_0$. For the atmosphere, this time is a few days; for the MODE region, assuming $L_0 = 60$ km and $V_0 = 5$ cm s^{-1}, this time is about 60 days. It is unlikely, therefore, that the much more rapidly developing modal coupling forecast deficiencies are due to turbulent unpredictability.

6. Summary

The essential results of this paper are as follows:

1) There exist significant barotropic and first baroclinic modal covariances: between both streamfunction and velocity fields; with positive values at zero spatial lag but with largest magnitudes at lag distances of approximately an eddy radius; most strongly associated with the lowest frequency mesoscale components; confirmed in independent data sets from MODE and, at least partly [i.e., $C_v(0) > 0$], from extended duration measurements at the MODE site; and occurring in such a configuration as to allow virtually no net energy transfer between the modes.

2) A variety of quasi-geostrophic two-mode model forecasts fail to adequately preserve these empirical modal relations, although some of the grosser aspects of mesoscale evolution (such as propagation rates or amplitude changes) are predicted moderately well. The failure of greatest dynamical consequence is the prediction of systematic transfers of energy from the baroclinic to the barotropic mode. This could lead to excessive barotropic energies in a long time integration, which in fact is an inadequacy reported by Owens and Bretherton (1978) for a related model, not run as a forecasting one.[4] This forecast failure appears to be insensitive to initial modal energy levels, initial data realization, mean vertical stratification strength, bottom topography, and the presence of similar eddies outside the MODE area (tested by shrinking the model periodicity length). It is therefore hypothesized that the mesoscale equilibrium balance in the MODE region, while characterized by zero modal energy transfer, is not an entirely local one in that the exterior regions provide a forcing influence which maintains the observed modal coupling.

Of course, it is not disproved by our forecast experiments that an exterior region which is initially statistically similar to the interior both in gross eddy characteristics and modal coupling relations would allow successful interior forecasts of the modal coupling relations; testing this requires creating artificial exterior data which goes beyond the scope of this study. Nevertheless, there is a pervasive tendency in the model forecast solutions to destroy $\epsilon \approx 0$. Also, the MODE region is located not in a large, statistically homogeneous part of the ocean but is adjacent to the relatively more energetic deep Gulf Stream gyre (Schmitz, 1977), whose mesoscale radiation might provide a forcing on the MODE region which influences the modal coupling. In conclusion, we are skeptical of the adequacy of an equilibrium, statistically homogeneous model of MODE mesoscale eddy modal coupling, even though such a model has performed well in other aspects (Owens and Bretherton, 1978).

3) The observational requirements for successful forecasting of the modal coupling relations appear to be quite great. From the MODE data, obtained at great effort by a large number of scientists, there

[4] Schmitz and Owens (1979) have qualified this statement of model inadequacy: for one frequency band (periods of 45–135 days) the modal energy ratios in the Bretherton and Owens model and the data agree well. A frequency decomposition is not available from the MODE data analyzed here.

remain significant uncertainties in the estimates of the observed modal relations, and their preservation in a plausible forecast model is only achieved with marginal credibility from the best initial realizations in a small interior region for a brief time. Whether the successor to MODE, POLYMODE, will have an adequate combination of both accuracy (resolution) and extensiveness remains to be seen. The most fruitful further investigations of the role of exterior region influence on modal coupling may be in models where various exterior processes can be arbitrarily specified.

Acknowledgments. Computational support for this work was given by Dr. Julianna Chow, secretarial support by Ms. Chris Kingsland, and financial support by the National Science Foundation through its grants to the National Center for Atmospheric Research (JCM) and the University of Washington, OCE 78-00559 (POLYMODE) (CYS).

REFERENCES

Bernstein, R. L., and W. B. White, 1974: Time and length scales of baroclinic eddies in the central North Pacific Ocean. *J. Phys. Oceanogr.*, **4**, 613–624.

Bernstein, R. K., 1974: Mesoscale ocean eddies in the North Pacific: Westward propagation. *Science*, **183**, 71–72.

Davis, R. E., 1975: Statistical methods. Dynamics and the Analysis of MODE-I: Report of the MODE-I Dynamics Group, Dept. of Meteorology, MIT, 250 pp.

——, 1977: Techniques for statistical analysis and prediction of geophysical fluid systems. *Geophys. Astrophys. Fluid Dyn.*, **8**, 245–277.

Flierl, G. R., 1978: Models of vertical structure and the calibration of two-layer models. *Dyn. Atmos. Ocean*, **2**, 341–381.

Freeland, H. J., P. B. Rhines and T. Rossby, 1975: Statistical observations of the trajectories of neutrally buoyant floats in the North Atlantic. *J. Mar. Res.*, **33**, 383–404.

Leith, C. E., and R. H. Kraichnan, 1972: Predictability of turbulent flows. *J. Atmos. Sci.*, **29**, 1041–1058.

Lorenz, E. N., 1969a: Three approaches to atmospheric predictability. *Bull. Amer. Meteor. Soc.*, **50**, 345–349.

——, 1969b: The predictability of a flow which possesses many scales of motion. *Tellus*, **21**, 289–307.

McWilliams, J. C., 1976: Maps from the Mid-Ocean Dynamics Experiment: Part I. Geostrophic streamfunction. *J. Phys. Oceanogr.*, **6**, 810–827.

——, and G. R. Flierl, 1975: Quasi-geostrophic wave analyses. Dynamics and the Analysis of MODE-I. Report of the MODE-I Dynamics Group, Dept. of Meteorology, MIT, 250 pp.

——, and ——, 1979: On the evolution of isolated, nonlinear vortices. *J. Phys. Oceanogr.*, **9**, 1155–1182.

——, and W. B. Owens, 1976: Estimation of spatial covariances from the MODE experiment. NCAR Tech. Rep. No. 115 + STR, 25 pp.

Owens, W. B., and F. P. Bretherton, 1978: Numerical simulation of mid-ocean mesoscale eddies. *Deep-Sea Res.*, **25**, 1–14.

Pochapsky, T. E., 1976: Vertical structure of currents and temperature in the western Sargasso Sea. *J. Phys. Oceanogr.*, **6**, 45–56.

Rhines, P. B., 1977: The dynamics of unsteady currents. *The Sea*, Vol. 6, Wiley, 189–318.

Richman, J. G., C. Wunsch and N. G. Hogg, 1977: Space and time scales of mesoscale motion in the sea. *Rev. Geophys. Space Phys.*, **15**, 385–420.

Rossby, H. T., 1974: Studies of the vertical structure of horizontal currents near Bermuda. *J. Geophys. Res.*, **79**, 1781–1791.

——, and T. B. Sanford, 1976: A study of velocity profiles through the main thermocline. *J. Phys. Oceanogr.*, **6**, 766–774.

Schmitz, W. J., 1977: On the deep general circulation in the western North Atlantic. *J. Mar. Res.*, **35**, 21–28.

——, 1978: Observations of the vertical distribution of low frequency kinetic energy in the western North Atlantic. *J. Mar. Res.*, **36**, 295.

——, and W. B. Owens, 1979: Observed and numerically simulated kinetic energies for some MODE eddies. *J. Phys. Oceanogr.*, **9**, 1294–1297.

Tarbell, S., and A. Spencer, 1978: A compilation of moored current data and associated observations (MODE-Site, 1971–1975). WHOI Tech. Rep., 78-5, Woods Hole, Mass.

Thompson, P. D., 1957: Uncertainty of initial state as a factor in the predictability of large-scale atmospheric flow patterns. *Tellus*, **9**, 275–295.